The FEBS Journal

FEBS PRESS science publishing by scientists

Absence of hexose-6-phosphate dehydrogenase results in reduced overall glucose consumption but does not prevent 11β-hydroxysteroid dehydrogenase-1-dependent glucocorticoid activation

Philippe Marbet, Petra Klusonova, Julia Birk, Denise V. Kratschmar and Alex Odermatt

Division of Molecular and Systems Toxicology, Department of Pharmaceutical Sciences, University of Basel, Switzerland

Keywords
11β-hydroxysteroid dehydrogenase; glucocorticoid; hexose-6-phosphate dehydrogenase; inflammation; macrophage

Correspondence
A. Odermatt, Division of Molecular and Systems Toxicology, Department of Pharmaceutical Sciences, University of Basel, Klingelbergstrasse 50, CH-4056 Basel, Switzerland
Fax: +41 61 207 1515
Tel: +41 61 207 1530
E-mail: alex.odermatt@unibas.ch

(Received 7 December 2017, revised 9 August 2018, accepted 21 August 2018)

doi:10.1111/febs.14642

Hexose-6-phosphate dehydrogenase (H6PD) is thought to be the major source of NADPH within the endoplasmic reticulum (ER), determining 11β-hydroxysteroid dehydrogenase 1 (11β-HSD1) reaction direction to convert inert 11-oxo- to potent 11β-hydroxyglucocorticoids. Here, we tested the hypothesis whether *H6pd* knock-out (KO) in primary murine bone marrow-derived macrophages results in a switch from 11β-HSD1 oxoreduction to dehydrogenation, thereby inactivating glucocorticoids (GC) and affecting macrophage phenotypic activation as well as causing a more aggressive M1 macrophage phenotype. *H6pd* KO did not lead to major disturbances of macrophage activation state, although a slightly more pronounced M1 phenotype was observed with enhanced proinflammatory cytokine release, an effect explained by the decreased 11β-HSD1-dependent GC activation. Unexpectedly, ablation of *H6pd* did not switch 11β-HSD1 reaction direction. A moderately decreased 11β-HSD1 oxoreduction activity by 40–50% was observed in *H6pd* KO M1 macrophages but dehydrogenation activity was undetectable, providing strong evidence for the existence of an alternative source of NADPH in the ER. *H6pd* KO M1 activated macrophages showed decreased phagocytic activity, most likely a result of the reduced 11β-HSD1-dependent GC activation. Other general macrophage functions reported to be influenced by GC, such as nitrite production and cholesterol efflux, were altered negligibly or not at all. Importantly, assessment of energy metabolism using an extracellular flux analyzer and lactate measurements revealed reduced overall glucose consumption in *H6pd* KO M1 activated macrophages, an effect that was GC independent. The GC-independent influence of H6PD on energy metabolism and the characterization of the alternative source of NADPH in the ER warrant further investigations.

Enzymes
11β-HSD1, EC 1.1.1.146; H6PD, EC 1.1.1.47.

Abbreviations
11-DHC, 11-dehydrocorticosterone; 11β-HSD1, 11β-hydroxysteroid dehydrogenase 1; BMDM, bone marrow-derived macrophages; CORT, corticosterone; DMEM, Dulbecco's modified eagle's medium; ECAR, extracellular acidification rate; ER, endoplasmic reticulum; G6P, glucose-6-phosphate; GC, glucocorticoid; GR, glucocorticoid receptor; H6PD, hexose-6-phosphate dehydrogenase; IFNγ, interferon-γ; IL, interleukin; iNOS, inducible nitric oxidase; KO, knock-out; LPS, lipopolysaccharide; MCP-1, monocyte chemoattractant protein-1; OCR, oxygen consumption rate; TNF-α, tumor necrosis factor-α; UHPLC–MS/MS, ultra-high-performance liquid chromatography–tandem mass spectrometry; WT, wild-type.

Introduction

Glucocorticoids (GC) essentially regulate major physiological functions, with potent modulatory effects on the immune system [1]. Besides the adrenal GC synthesis, the tissue- and cell-specific interconversion of active 11β-hydroxy GC [cortisol in human, corticosterone (CORT) in rodents] and inactive 11-oxo GC [cortisone in human, 11-dehydrocorticosterone (11-DHC) in rodents] by 11β-HSD enzymes plays an important role in mediating GC effects [2]. Two isozymes are known, 11β-HSD2 converts 11β-hydroxy to 11-oxo GC and 11β-HSD1 catalyzes *in vivo* the reverse reaction. 11β-HSD1 is a bidirectional enzyme facing the endoplasmic reticulum (ER) lumen, where it interacts with hexose-6-phosphate dehydrogenase (H6PD) [3–6]. H6PD utilizes glucose-6-phosphate (G6P) to produce NADPH in the ER [7,8]. As the ER membrane is not permeable for pyridine nucleotides, the intraluminal regeneration of NADPH by H6PD determines 11β-HSD1 to predominantly catalyze the oxoreduction of 11-oxo GC [4,9]. Upon disruption of the cell membrane in homogenized cells or tissue, the intraluminal NADPH is rapidly metabolized and in the absence of G6P this results in a loss of oxoreduction activity. A switch from oxoreduction to dehydrogenation activity was observed when comparing 11β-HSD1 activity in liver microsomes of wild-type (WT) and *H6pd* knock-out (KO) mice, and the urinary excretion revealed a dramatic shift in the 11-oxo/11β-hydroxy GC ratio [10]. H6PD is currently the only well characterized enzyme within the ER that generates NADPH and it is thought to be responsible for maintaining a high luminal NADPH/$NADP^+$ ratio. Therefore, we anticipated that in cells from *H6pd* KO mice 11β-HSD1 would catalyze predominantly the dehydrogenation reaction, thereby inactivating GC.

Glucocorticoids affect cells of the immune system and impact gene expression, enzymatic activity, and cellular differentiation and migration [11]. GC are, for example, crucial for T-cell selection by regulating apoptosis. In macrophages, they play a pivotal but not yet fully elucidated role in the phenotypic activation [12], and they suppress the expression and secretion of proinflammatory cytokines such as interleukin-1β (IL-1β), interleukin-6 (IL-6), interferon-γ (IFNγ), and tumor necrosis factor-α (TNF-α), thereby preventing an overshooting immune response [13–16]. Blood monocytes, derived from bone marrow progenitor cells, are constantly patrolling the blood vessels, fulfilling various functions in both innate and adaptive immunity. If activated by tissue damage or infection, they enter the affected tissue and undergo phenotypic activation. Depending on the type of activator, the classically activated M1 and the alternatively activated M2 macrophages are distinguished. IFNγ, TNF-α, or lipopolysaccharide (LPS) induce a M1 phenotype producing proinflammatory cytokines and bactericidal mediators, whereas interleukin-4 (IL-4) or interleukin-13 (IL-13) result in an M2 phenotype contributing to the downregulation of inflammation and elimination of tissue debris [17–21].

The expression of 11β-HSD1 in patrolling monocytes is absent or very low, but strongly induced upon activation toward a M1 phenotype [22]. It has been shown that 11β-HSD1 is regulated dynamically during an ongoing inflammation, which is crucial for a controlled and rapid resolution of inflammation since GC restrain the M1 activated macrophages and promote a M2 phenotype [23,24]. Additionally, an increased 11β-HSD1 oxoreduction activity was hypothesized to cause a re-routing of the H6PD substrate G6P toward the ER, causing a change in overall glucose metabolism that has been shown to alter macrophage polarization [25,26].

In the present study, we investigated whether in bone marrow-derived macrophages (BMDM) from *H6pd* KO mice 11β-HSD1 would predominantly function as a dehydrogenase, thereby inactivating GC and resulting in enhanced expression of proinflammatory cytokines. Furthermore, we tested whether the decreased 11β-HSD1-dependent GC activation due to absence of H6PD activity would affect the activation of macrophage phenotypes and their functions. We found that ablation of *H6pd* did not cause a loss of GC activation by 11β-HSD1 but only a reduction by 40–50%, which translated into a decreased suppression by 11-DHC of proinflammatory cytokine expression. General macrophage functions were only moderately influenced and the *H6pd* KO only led to slightly exaggerated M1 activation state with a marginally increased proinflammatory cytokine release. However, the KO of *H6pd* did cause an overall increased glucose consumption and lactate secretion, most likely by a GC-independent mechanism.

Results

Decreased glucocorticoid activation in H6pd KO M1 macrophages

Based on earlier observation of an almost complete loss of 11β-HSD1 oxoreduction activity in liver microsomes isolated from *H6pd* KO mice [10], we expected a loss of the oxoreduction activity in BMDM from *H6pd* KO mice and that the enzyme would

predominantly exhibit oxidation activity. To test this assumption, WT and *H6pd* KO M1 macrophages were incubated with 100 nM 11-DHC for 24 h, followed by determination of the amount of CORT released into the medium by ultra-high-performance liquid chromatography–tandem mass spectrometry (UHPLC-MS/MS). Surprisingly, compared to WT, *H6pd* KO macrophages still retained 50–60% of the oxoreduction activity (Fig. 1A). Treatment of the macrophages with the 11β-HSD1 inhibitor BNW16 [27] fully abolished the oxoreduction activity in both WT and *H6pd* KO macrophages, confirming that this activity was indeed 11β-HSD1-specific.

Diminished suppressive effect of 11-DHC on proinflammatory cytokine expression in H6pd KO M1 macrophages

To assess the functional impact of the altered 11β-HSD1 activity, macrophages were activated toward an M1 phenotype for 24 h followed by 24 h incubation with increasing concentrations of 11-DHC, which requires oxoreduction by 11β-HSD1 to CORT in order to exert a suppressive effect on the expression of proinflammatory cytokines. Hence, the decrease in proinflammatory cytokine mRNA expression can serve as a functional readout of the 11β-HSD1 oxoreduction activity. Unlike initially anticipated, only moderate effects were observed in the *H6pd* KO macrophages. While treatment with 11-DHC suppressed the expression of all four cytokines measured, only *Mcp-1* and *Il-1*β mRNA expression in WT macrophages tended to show a more pronounced decrease at 100 and 1000 nM 11-DHC compared with *H6pd* KO macrophages, in line with higher 11β-HSD1 oxoreduction activity in WT macrophages (Fig. 1B,C). Preincubation of cells for 24 h with 100 nM 11-DHC followed by activation into M1 phenotype with LPS+IFNγ did not result in significant changes of *Il1*-β, *Mcp1*, *Il-6*, and *Tnf*α mRNA expression when comparing either pretreated WT and KO cells or when comparing pretreated and untreated cells at 1, 2, 4, 8, or 24 h after stimulation (data not shown).

Impact of H6pd KO on macrophage phenotypes

To examine whether the observed difference in 11β-HSD1 activity and the reduced ability of the *H6pd* KO macrophages to decrease proinflammatory markers has an impact on macrophage phenotypic

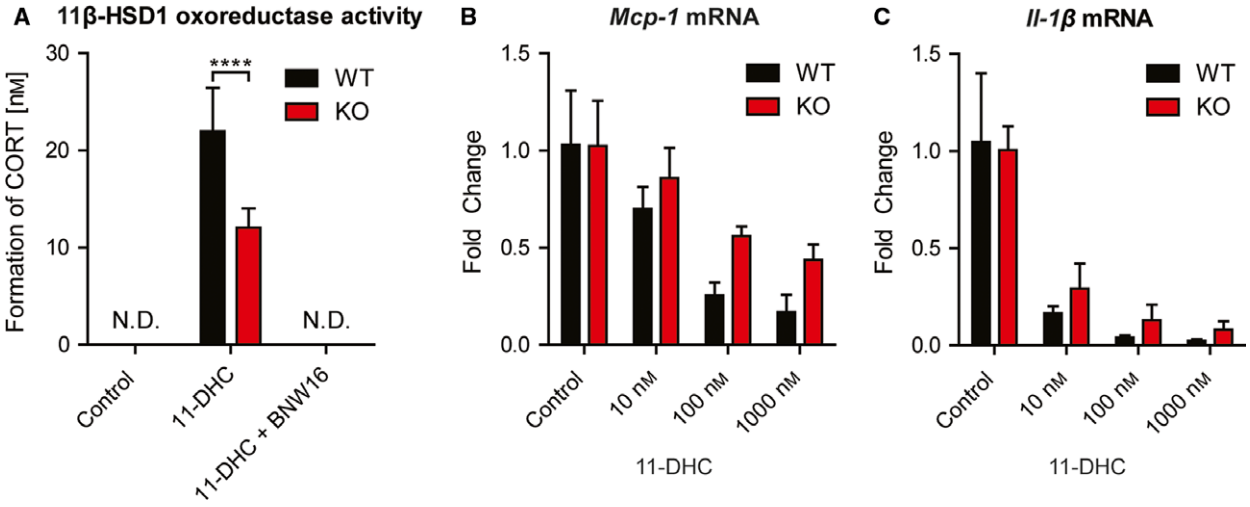

Fig. 1. Conversion of 11-DHC to CORT in WT and *H6pd* KO macrophages and effect on proinflammatory cytokine expression. (A) M1 polarized macrophages from WT and *H6pd* KO mice were incubated with 100 nM 11-DHC for 24 h and formation of CORT was determined in the supernatants by UHPLC-MS/MS. 11β-HSD1 was inhibited by 1 h preincubation with 1 μM BNW16. *H6pd* KO macrophages retained 50–60% 11β-HSD1 oxoreduction activity and inhibition of 11β-HSD1 completely abolished the formation of CORT in both WT and *H6pd* KO macrophages (mean ± SD from two animals performed in quadruplicates). Data were analyzed using the Shapiro–Wilk normality test and unpaired *t*-test (B, C) After 24 h of M1 phenotypic activation, WT and *H6pd* KO macrophages were treated with increasing concentrations of 11-DHC for 24 h and expression of proinflammatory markers was measured by real-time PCR. mRNA expression of *Mcp-1* (B) and *Il-1*β (C) showed a significant larger decrease in WT than in *H6pd* KO macrophages at 100 and 1000 nM and a trend at 10 nM. Results were normalized to the house-keeping gene *Ppia* and reported as fold change compared to control (mean ± SD of 2 WT and 3 KO animals performed in duplicates). (B, C) Data were analyzed using the Shapiro–Wilk test and the Kruskal–Wallis test followed by the Dunn's posttest. CORT; 11-DHC; N.D. (not detectable); ****$P < 0.0001$.

activation, the mRNA expression levels of phenotype-specific marker genes and other genes of interest were qualitatively assessed in M0, M1, and M2-polarized macrophages from 8- to 12-week-old mice by real-time PCR. Besides *H6pd*, which is clearly expressed in WT but not *H6pd* KO macrophages, the phenotype markers indicated a trend toward a more pronounced M1 phenotype in *H6pd* KO macrophages (Fig. 2A). The overall phenotypic activation seemed to be maintained; the M1 macrophages highly expressed all M1-specific markers, for example, *iNos*, *Mcp1*, *Il1*-β, *Tnf*α, and *Il-6*, whereas the M2 macrophages expressed M2-specific markers such as *Cd206*, *Ym1*, and *Fizz1*. This shows that the absence of *H6pd* had only a minor impact on macrophage phenotypic activation. The glucocorticoid receptor (GR) was highly expressed in all phenotypes, whereas *11*β-*hsd1* mRNA was upregulated in the M1 activation state but hardly expressed in M0 and M2 macrophages. Therefore, further experiments focused on M1 activated macrophages.

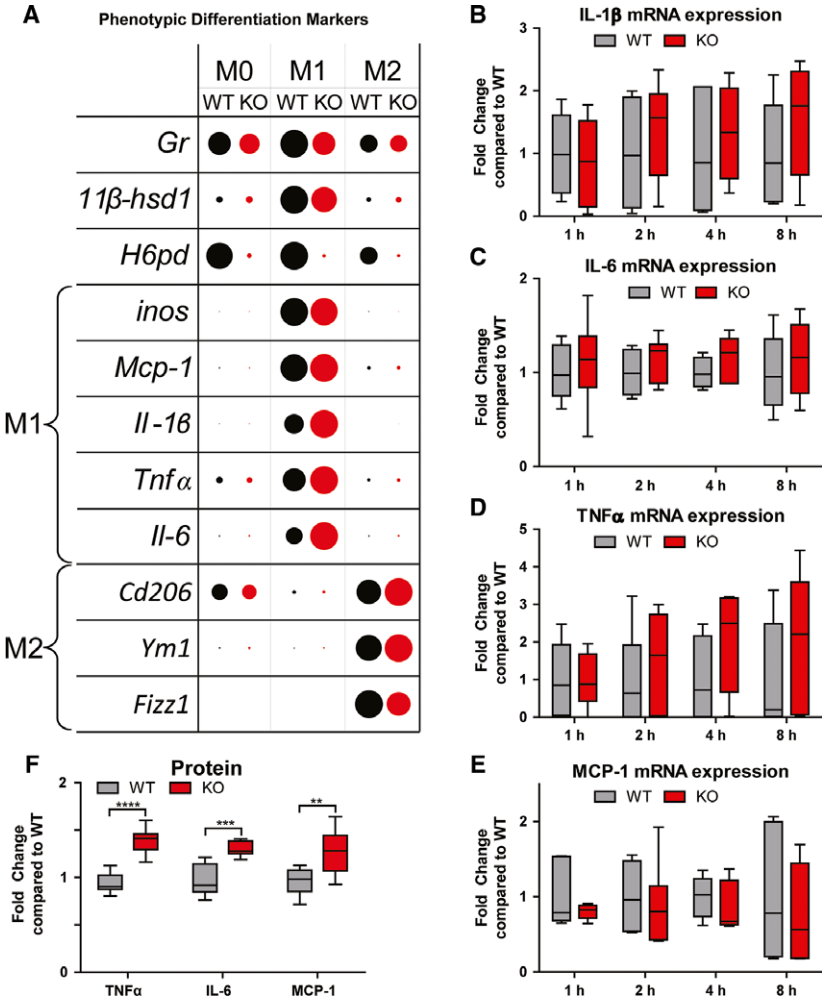

Fig. 2. Confirmation of general phenotypes and comparison of M1 polarization in WT and *H6pd* KO macrophages. (A) For a qualitative assessment, the mRNA expression of various markers of M1 and M2 activation state were analyzed in M0, M1 and M2 macrophages isolated from 8- to 12-week-old WT and *H6pd* KO mice using real-time PCR. For each gene, the spot area is directly proportional to the fold change in mRNA abundance compared to the WT M0 macrophages. The largest spot (highest expression) in each row was set to a fixed arbitrary size. The absence of *H6pd* did not cause major changes in macrophage phenotypic activation (mean of 5–8 KO mice and 5–8 WT mice). (B–E) Macrophages 6 WT and 6 *H6pd* KO mice were activated toward a M1 phenotype and expression of M1-specific mRNA markers were measured after 1, 2, 4, and 8 h using real-time PCR. (F) Cytokines in the supernatant were measured after 4 h of M1 phenotypic induction using ELISA. The absence of *H6pd* caused significantly increased secretion of TNFα, IL-6 and MCP-1 protein (mean ± SD of 2 WT and 3 KO animals measured in duplicates). (B-F) Data were analyzed using the Shapiro–Wilk normality test and one-way ANOVA. N.D. (not detectable); $^{**}P < 0.01$; $^{***}P < 0.001$; $^{****}P < 0.0001$.

A time-course covering the initial burst phase was performed in WT and *H6pd* KO M1 macrophages and their M1 marker expression levels were compared at different time-points (Fig. 2B–E). Although *Tnf*α and *Il-1*β mRNA expression levels showed a trend toward increased expression in *H6pd* KO compared to WT macrophages, they were not significantly altered at any time point. Similar results were obtained when comparing non-elicited peritoneal macrophages isolated from WT and *H6pd* KO mice activated toward an M1 phenotype, where only *Tnf*α showed a trend toward an increase in *H6pd* KO compared to WT (data not shown).

To assess the biological relevance of the observed trends in some M1 markers, secreted protein levels were measured. Therefore, M0 cells were incubated with LPS and IFNγ for 4 h to induce the M1 activation state, followed by analysis of cell supernatants by ELISA. This revealed an approximately 1.4-fold higher secretion of monocyte chemoattractant protein-1 (MCP-1), IL-6 and TNFα proteins in *H6pd* KO compared to WT macrophages (Fig. 2F).

Impact of H6pd KO on general properties of M1 macrophages

Next, the impact of *H6pd* KO on typical M1 macrophage functions, such as phagocytosis, nitrite production, and cholesterol efflux, was examined. Nitrite production, mainly mediated by the inducible nitric oxidase (iNOS), was measured using the Griess assay. No nitrite production could be detected in supernatants of M0 and M2 cells, which is in agreement with the background levels of *iNos* mRNA expression in these phenotypes; however, it was well detectable in M1 macrophages, with a small but statistically significant decrease in *H6pd* KO cells (Fig. 3A). The

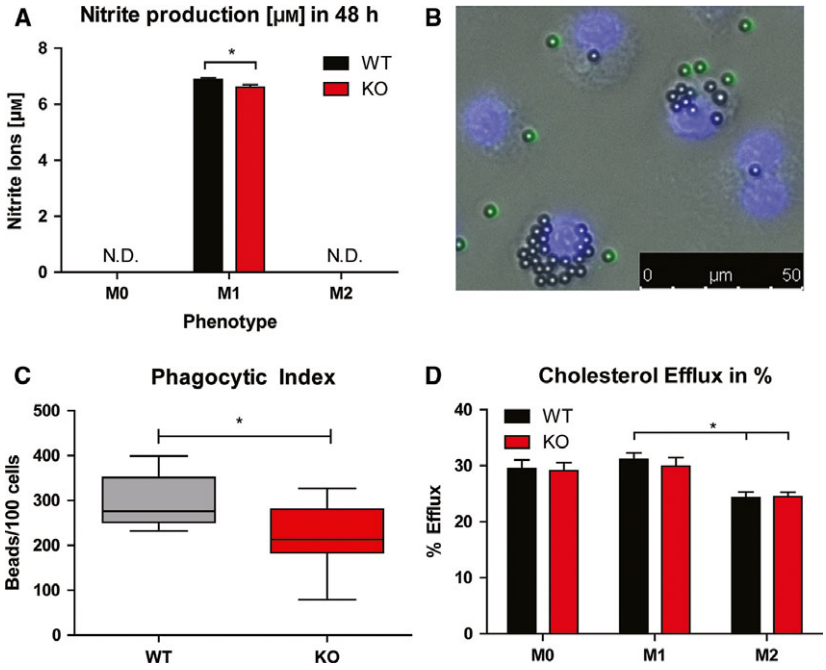

Fig. 3. Comparison of general functions in WT and *H6pd* KO macrophages. (A) Production of nitrite was measured using Griess reagent in supernatants of M0, M1, and M2 macrophages following 48 h of incubation. *H6pd* KO M1 macrophages showed a slightly decreased nitrite production compared to WT cells, whereas nitrite production was not detectable in supernatants of M0 or M2 macrophages. (B) Fluorescent microscopy picture of phagocytosis of opsonized latex beads by M1 macrophages. (C) Comparison of phagocytotic activity in WT and *H6pd* KO M1 macrophages. Cells were incubated for 10 min with IgG ALEXA-594 labeled beads and fixed with paraformaldehyde. Nuclei were stained with Hoechst-33342 (blue) and external beads were labelled with IgG ALEXA-488 (green). Phagocytic activity of M1 macrophages from WT and *H6pd* KO mice was assessed as the number of beads per 100 cells from pictures taken of each well. Scale bar: 20 µm. (D) Assessment of cholesterol efflux by WT and *H6pd* KO macrophages. M0, M1, and M2 macrophages were incubated with [^{3}H]-cholesterol for 48 h. Upon equilibration, cholesterol efflux was determined after 4 h by analyzing [^{3}H]-cholesterol in supernatants and cells by liquid scintillation counting. The percentage of efflux was calculated as fraction of [^{3}H]-cholesterol in supernatant compared to that of medium plus cells. Data represent mean ± SD from three animals, performed in triplicates (A, C), analyzed by the Shapiro–Wilk and unpaired *t*-test, or mean ± SD of four measurements (D) analyzed by the Shapiro–Wilk and Kruskal–Wallis test followed by the Dunn's posttest. N.D. (not detectable), $*P < 0.05$.

assessment of the phagocytic activity, a key function of macrophages, by counting the number of IgG opsonized latex beads taken up by 100 cells during the 10 min incubation period (Fig. 3B), revealed a significantly reduced phagocytic index in *H6pd* KO M1 macrophages (Fig. 3C). Cholesterol efflux, another important function of macrophages, was measured in all phenotypes using [^{3}H]-cholesterol and was calculated as the percentage of radioactivity in the medium from total radioactivity in medium plus cells. No difference could be detected between WT and *H6pd* KO macrophages (Fig. 3D). Thus, *H6pd* KO decreased phagocytic activity and had a modest effect on nitrite production, but did not affect cholesterol efflux.

Decreased glycolytic capacity in H6pd-deficient M1 macrophages

To investigate whether *H6pd* deficiency affects metabolic parameters that affect macrophage function, a glycolysis stress test was performed using a Seahorse XFp analyzer. Thereby, compounds targeting key elements of cellular metabolism are sequentially added at indicated time points. In the first injection, glucose was added as an energy source. Next, oxidative phosphorylation in the mitochondria was shut down by adding oligomycin and forcing the cells to cover their energy demand exclusively by glycolysis. Finally, 2-deoxyglucose was added to inhibit glycolysis by blocking glucose hexokinase and verifying glycolysis as a major source of the previously measured basal extracellular acidification rate (ECAR). During this procedure, the ECAR and oxygen consumption rate (OCR) are measured in a transient microchamber. The ECAR measurements showed a decreased baseline glycolytic activity in *H6pd* KO compared to WT M1 macrophages (Fig. 4A–C). In both WT and *H6pd* KO macrophages, the glycolytic reserve, indicated by the increase in ECAR upon addition of oligomycin, was low, pointing toward a negligible role of mitochondrial energy production. The OCR was also lower in *H6pd* KO compared to WT M1 macrophages under glucose deprivation (Fig. 4D–F). This difference was less pronounced upon addition of glucose, whereby the *H6pd* KO macrophages seemed to have lost the responsiveness to glucose addition. The nonresponsiveness in the OCR measurements is characteristic of M1 activated macrophages and represents a state of inhibited mitochondrial oxidative respiration [28]. To confirm the decreased acidification rates of the *H6pd* KO macrophages measured in the Seahorse analyzer by another approach, lactate levels were determined using a colorimetric assay kit. M0 macrophages of WT and *H6pd* KO were activated toward an M1 phenotype while supernatant samples were taken at 4, 24, and 48 h. The amount of lactate produced in *H6pd* KO macrophages showed a weak trend toward a decrease after 24 h, which became significant after 48 h (Fig. 4G).

Discussion

In this study, we showed that the loss of *H6pd* in macrophages unexpectedly did not abolish 11β-HSD1-dependent conversion of 11-DHC to CORT but resulted in a rather moderate decrease of oxoreduction activity of only 40–50%. Dehydrogenation activity could neither be detected in intact WT nor in *H6pd* KO macrophages. The fact that there is no switch from 11-oxoreduction to dehydrogenation in *H6pd* KO macrophages as well as the moderate decrease in oxoreduction activity is surprising and might be explained by a compensatory adaptation involving a yet unknown NADPH generating system in the ER. Results from HEK-293 cells transfected with *H6pd* compared to mock transfected cells and data from HT-1080 connective tissue cells where *H6pd* was knocked down using siRNA showed a switch from 11β-HSD1 oxoreduction to dehydrogenation activity when *H6pd* was absent or knocked down [3,4,29]. These cell types might not express the alternative NADPH generating system present in the ER of macrophages. Also, studies with liver microsomes from *H6pd* KO mice showed an almost complete loss of oxoreduction but high dehydrogenation activity [10]. Notably, NADPH is not freely passing the ER membrane and during preparation of microsomes, the NADPH in the luminal compartment is used up because of the absence of the substrate for the luminal NADPH regenerating system (i.e. G6P for H6PD or the substrate of the yet unknown luminal regenerating system).

Currently, H6PD represents the only well characterized enzyme generating NADPH in the ER and based on the observation of an almost complete loss of 11β-HSD1 oxoreduction activity in liver microsomes from *H6pd* KO mice it was suggested that H6PD is the major source of NADPH within the ER [10]. Our observation of a rather moderate effect of *H6pd* KO on 11β-HSD1 oxoreduction activity in intact macrophages indicates the existence of an alternative yet less efficient source for NADPH in the ER of these cells. The distinct effect of H6PD deficiency in macrophage, HT-1080 and HEK-293 cells suggests a cell-type specific expression of such an alternative NADPH regenerating system in the ER.

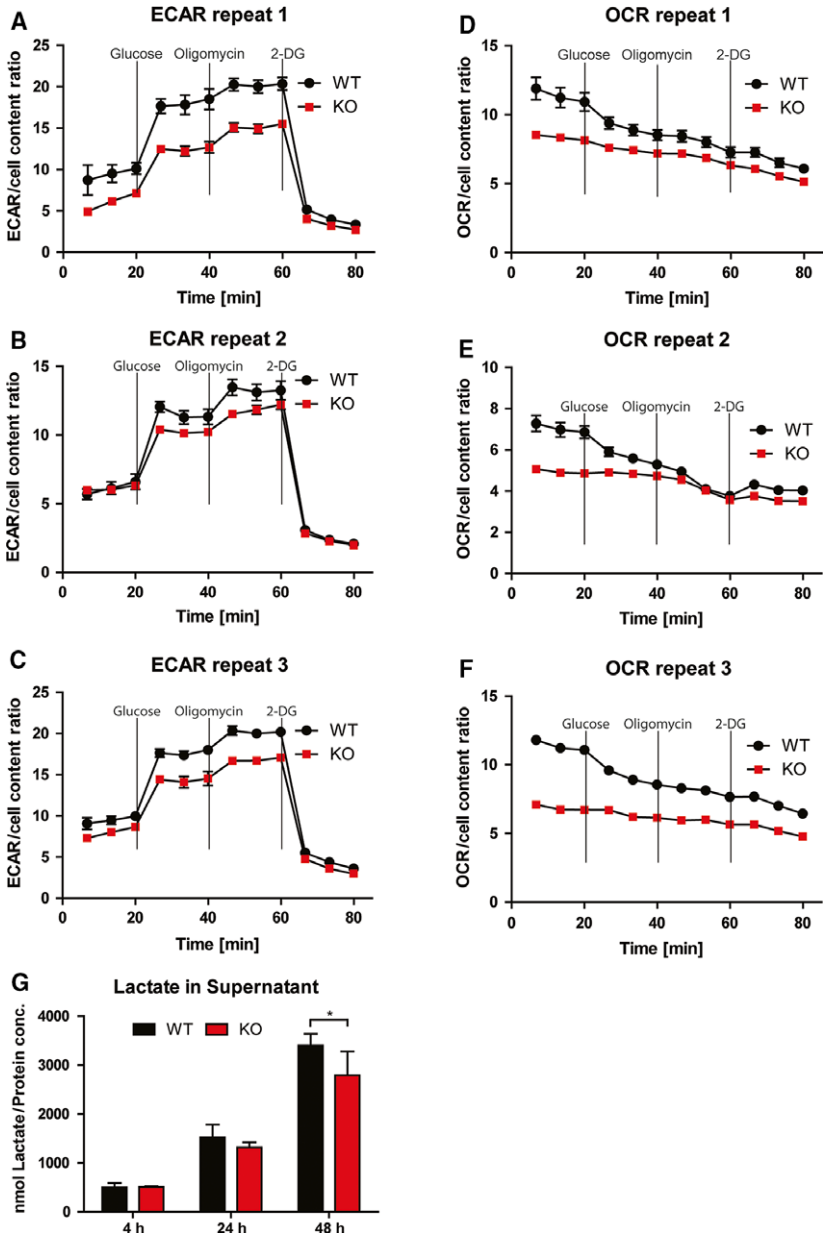

Fig. 4. Assessment of metabolic parameters of WT and *H6pd* KO M1 macrophages. Basal ECAR, A–C) and oxidation consumption rates (OCR, D–F) were recorded in a Seahorse XFp Extracellular Flux Analyzer, followed by the sequential addition of 10 mM glucose, 1 μM oligomycin, and 50 mM 2-deoxyglucose (2-DG). *H6pd* KO macrophages showed lower basal ECAR and OCR and an overall decreased ECAR (mean ± SD of three measurements). (G) M1 macrophages of WT and *H6pd* KO were incubated and the amount of lactate was measured at 4, 24 and 48 h using a colorimetric lactate assay kit. H6PD KO macrophages showed decreased lactate production after 48 h. Values were normalized to protein content (mean ± SD of three animals measured in duplicates). Data were analyzed by Shapiro–Wilk and one-way ANOVA $*P < 0.05$.

Earlier work provided evidence for the existence of a pentose phosphate pathway in the ER [30], whereby H6PD was shown to catalyze the first two steps of this pathway, converting G6P to 6-phosphogluconate [31]. There is evidence from work on liver microsomes for the existence of a 6-phosphogluconate dehydrogenase in the ER that produces NADPH ([32,33], own observations); however, the corresponding gene remains to be identified. Nevertheless, as 6-phosphogluconate is not freely permeable across the ER membrane, this enzyme unlikely accounts for the observed remaining 11β-HSD1-dependent oxoreduction activity. The unknown source of NADPH in the ER needs to be uncovered, and *H6pd* KO macrophages constitute an interesting model for studying such mechanisms.

Interestingly, the absence of *H6pd* did not grossly interfere with macrophage activation into M1 and M2 phenotypes. Due to the moderate effect of *H6pd* KO on 11β-HSD1 oxoreduction activity, the M1 phenotype was barely affected, with only weak trends toward an increased expression of some M1 markers and an approximately 1.4-fold increased release of proinflammatory cytokines, most likely because of lower production of active GC. Considering the great

inducibility of macrophage cytokine expression and secretion, these minor changes are unlikely to be of biological relevance. A more strongly enhanced release of proinflammatory cytokines was reported in 11β-HSD1-deficient mice [23,34]. Whereas M1 macrophages from *H6pd* KO mice showed comparable 11β-HSD1 expression to WT cells, the corresponding oxoreduction activity was reduced. This is in agreement with the above-mentioned regulation of 11β-HSD1 activity via cosubstrate availability. Thus, regarding GC activation the alternative NADPH source could not entirely compensate for the loss of *H6pd*, resulting in a weak trend toward a more pronounced M1 phenotype.

Other general macrophage functions, including cholesterol efflux and nitrite production, were not changed or were statistically significant but not considered biologically relevant, respectively. In the *H6pd* KO macrophages, the moderate effect on 11β-HSD1 was not sufficient to affect cyclodextrin-stimulated cholesterol efflux. This may seem surprising because in macrophages from *11β-hsd1*-deficient mice an increase in ApoAI-stimulated cholesterol efflux was reported [35]. A possible explanation may be that overall cholesterol efflux was measured using cyclodextrin as cholesterol acceptor, which is not pathway specific, whereas ApoAI exclusively stimulates ABCA1-dependent efflux.

Furthermore, it was shown that GC promote phagocytic activity of macrophages and that the higher phagocytic activity of macrophages upon treatment with 11-DHC is dependent on 11β-HSD1 [23]. 11β-HSD1 was found to promote the rapid clearance of apoptotic leukocytes during the resolution of inflammation, whereby phagocytic clearance was delayed in macrophages from *11β-hsd1* KO mice. Whether the observed decrease in phagocytic activity of *H6pd* KO macrophages, most likely a consequence of the lower GC activation due to the limited supply of NADPH as 11β-HSD1 substrate, results in delayed phagocytic clearance and resolution of inflammation *in vivo* remains to be investigated.

Besides its role in GC activation, H6PD may affect other metabolic functions through catalyzing the first two steps of the pentose phosphate pathway in the ER [36]. The present analysis of the metabolism of M1 macrophages showed that they cover their energy demand almost exclusively through aerobic glycolysis. This is in agreement with the generally accepted Warburg-like metabolism found in dendritic cells and in macrophages upon LPS stimulation [37]. Noteworthy, the *H6pd* KO macrophages showed a markedly decreased overall glucose consumption, further consolidated by a decreased lactate concentration in cell supernatants. Such a decrease was also reported in cancer cells upon knock-down of *H6pd* and attributed to a H6PD-dependent glucose utilization pathway [38]. Additional support for the contribution of such a pathway comes from the increased OCR under glucose starvation observed in WT macrophages in the present study. The effect of using oxygen despite being primed for aerobic glycolysis has also been reported for T cells under glucose-starved conditions [39]. Since the *H6pd* KO macrophages show less oxygen consumption under these conditions, they seem to be less affected by the limited availability of glucose due to their reduced overall glucose consumption.

In conclusion, we showed that *H6pd* KO does not lead to major disturbances of macrophage phenotypic activation and that it results in only a moderate decrease in 11β-HSD1-mediated GC activation in M1 macrophages and not to a switch of this enzyme to primarily catalyze the oxidation reaction. *H6pd* KO M1-polarized macrophages showed only a slight trend toward a more aggressive M1 phenotype but displayed a significantly reduced phagocytic activity, in agreement with decreased GC activation. Importantly, *H6pd* KO M1 macrophages showed decreased glucose utilization and lactate production rates, most likely by a GC-independent mechanism. The results indicate a modulatory role of H6PD in 11β-HSD1-dependent GC activation as well as a GC-independent role in regulating energy metabolism.

Methods

Generation of bone marrow-derived macrophages and activation to M1 and M2 phenotype

Bone marrow-derived macrophages were obtained from femurs of female C57BL/6 WT and *H6pd* KO mice at the age between 10 and 12 weeks as described previously [40]. The *H6pd* KO mouse line was kindly provided by Gareth Lavery, University of Birmingham, UK [10]. Mice were housed in climate-controlled facility under standard conditions on a 12 h light/12 h dark cycle with free access to standard chow and drinking water. The mice were sacrificed by CO_2, followed by isolation of BMDM. All procedures were approved by the Cantonal Veterinary Office in Basel, Switzerland. After cervical dislocation both femurs were dissected and the epiphyses removed. The bone marrow was flushed into a 15-mL plastic tube with 8 mL Dulbecco's modified Eagle's medium (DMEM, Sigma-Aldrich, St. Louis, MO, USA) using a 25-G needle on a syringe. Upon centrifugation at 200 × ***g*** for 2 min the pellet was resuspended in 800 μL DMEM

supplemented with 10% FBS (Connectorate, Dietikon, Switzerland), 100 $U \cdot mL^{-1}$ penicillin, 100 $\mu g \cdot mL^{-1}$ streptomycin, followed by distribution into eight 6-cm bacterial dishes containing 5 mL of the same medium supplemented with 10 $ng \cdot mL^{-1}$ macrophage colony-stimulating factor (BioLegend, San Diego, CA, USA). Cells were then incubated at 5% CO_2 and 37 °C in order to induce differentiation into BMDM. After 3 days, 5 mL of new medium was added. Cells were harvested at day 7 by scraping.

Phenotypic activation of BMDM was induced by supplementing the differentiation medium with 100 $ng \cdot mL^{-1}$ LPS and 50 $ng \cdot mL^{-1}$ IFNγ for M1 phenotype, and 10 $ng \cdot mL^{-1}$ IL-4 (cytokines were from Sigma-Aldrich) for M2 phenotype. The incubation time was 4 h in case of cytokine secretion measurements and 24 h for functional assays.

Gene expression analysis by real-time polymerase chain reaction

Total RNA was isolated from BMDM using TRI® Reagent (Sigma-Aldrich) and purified with the Direct-zol™ RNA MiniPrep kit (Zymo Research, Irvine, CA, USA) according to the manufacturer's protocol. Moloney murine leukemia virus reverse transcriptase (M-MLV-RT, Promega, Fitchburg, WI, USA) was used for cDNA synthesis. KAPA SYBR® Fast qPCR Master Mix (KAPA Biosystems, Woburn, MA, USA) was used for the RT-PCR comprising 40 cycles of 95 °C for 10 s, 60 °C for 15 s, followed by a final extension at 72 °C for 20 s, and a dissociation curve. The oligonucleotide primers (Table 1) were designed using the IDT SciTool for real-time PCR and synthesized by Microsynth® (Balgach, Switzerland).

Quantification of steroids in cell culture supernatants

To each culture supernatant or calibrator (100 μL) an internal standard solution containing corticosterone-d8 in acetonitrile (100 μL, 200 nM) was added. Proteins were precipitated by adding ice-cold acetonitrile (500 μL) and samples were incubated thoroughly shaking (20 min, 1300 r.p.m., 4 °C). Samples were centrifuged (10 min, 16 000 × ***g***, 4 °C). Samples were evaporated to dryness and reconstituted in methanol (25 μL, 15 min, 1300 r.p.m., 4 °C). CORT and 11-DHC were quantified by UHPLC–MS/MS using an Agilent 1290 UHPLC coupled to an Agilent 6490 triple quadrupole mass spectrometer essentially as described earlier [41].

Griess assay

Free nitrite was measured in culture supernatants using Griess reagent (Sigma-Aldrich). BMDM were seeded at a density of 0.5×10^6 cells/well in a non-tissue culture treated 12-well plate (Starlab, Switzerland) and activated toward M1 or M2 phenotypes or left in their unactivated state in phenol red-free medium for 48 h. A quantity of 100 μL of supernatant was transferred in triplicates onto a 96-well plate. Then, 100 μL of Griess reagent was added, the plate incubated for 5 min at 37 °C, followed by measuring the absorbance at 540 nm. The results were normalized to total protein content, determined by using the Pierce BCA protein assay according to the manufacturer's protocol (Thermo Fisher Scientific, Waltham, MA, USA).

Determination of phagocytic index

The phagocytic index was determined as described previously [42]. Briefly, polystyrene latex beads with 3 μm mean particle size (Sigma-Aldrich) were opsonized with anti-goat IgG (Sigma-Aldrich) and labeled with donkey anti-goat IgG ALEXA-594 (Life Technologies, Zug, Switzerland). BMDM were seeded at a density of 0.5×10^5 cells/well on a 96-well plate and left in M1 differentiation medium for 24 h. A quantity of 100 μL of opsonized and labeled bead-solution was added to each well and the plate was

Table 1. Primer sequences

	Forward	Reverse
Ppia	CAAATGCTGGACCAAACACAAACG	GTTCATGCCTTCTTTCACCTTCCC
Gr	TGCTATGCTTTGCTCCTGATCTG	TGTCAGTTGATAAAACCGCTGCC
11β-hsd1	TGGTGCTCTTCCTGGCCTACT	CCCAGTGACAATCACTTTCTTT
H6pd	CTTGAAGGAGACCATAGATGCG	TGATGTTGAGAGGCAGTTCC
inos	ATGAGGTACTCAGCGTGCTCCA	CCACAATAGTACAATACTACTT
Mcp-1	TTAAAAACCTGGATCGGAACCAA	GCATTAGCTTCAGATTTACGGGT
Il-1β	CAACCAACAAGTGATATTCTCCATG	GATCCACACTCTCCAGCTGCA
Tnfα	CTTCTGTCTACTGAACTTCGGG	TGTCTTTGAGATCCATGCCG
Il-6	TCCAGTTGCCTTCTTGGGAC	AGTCTCCTCTCCGGACTTGT
Cd206	CTCTGTTCAGCTATTGGACGC	TGGCACTCCCAAACATAATTTGA
Ym1	GATGCAGAACAATGAGATCACC	ATGGTAGTGAAAGGAGCAGTTC
Fizz1	AAGCCTACACTGTGTTTCCTTTT	GCTTCCTTGATCCTTTGATCCAC

centrifuged at 350 × ***g*** for 1 min for synchronized settling of beads. After 10 min at 37 °C, phagocytosis was arrested by placing the plate on ice and washing twice with cold medium. Remaining external particles were labelled by adding donkey anti-goat IgG ALEXA-488 (Life Technologies) for 5 min. After fixation with 4% paraformaldehyde and staining with Hoechst-33342 (Invitrogen, Carlsbad, CA, USA) cells were covered with PBS. Cells of five random fields per well were manually analyzed using a Leica DMI 4000B fluorescence microscope. The phagocytic activity was assessed as number of beads/100 cells from four independent measurements.

Measurement of cholesterol efflux

Cholesterol efflux was measured as described previously [43]. Briefly, BMDM were seeded at a density of 0.4×10^6 cells/well of a 12-well plate and either activated toward an M1 or M2 phenotype or left in the M0 state. Cells were incubated in medium containing 0.5 $\mu Ci \cdot mL^{-1}$ [^{3}H]-cholesterol (PerkinElmer, Boston, MA, USA) for 48 h, the medium was removed and cells were washed twice with prewarmed PBS. Serum-free medium was added for 18 h to allow equilibration of the labeled cholesterol between the cellular compartments. Cells were washed and incubated with new serum-free medium in the absence or presence of 1 $mg \cdot mL^{-1}$ cyclodextrin (Sigma-Aldrich) as a cholesterol efflux acceptor for 4 h. The [^{3}H]-cholesterol efflux was then quantified by separate liquid scintillation counting of supernatant and cell lysate and reported as the ratio of radiolabeled cholesterol in the medium compared to that of medium and cells.

ELISA

Bone marrow-derived macrophages were seeded at a density of 0.5×10^6 cells/well in a 12-well plate and allowed to settle for 24 h. Then, BMDM were activated toward an M1 phenotype for 4 h, followed by collecting supernatants, and measuring TNFα, IL-1β, and MCP-1 levels using an ELISA Ready-SET-Go kit according to the manufacturer's protocol (eBioscience, San Diego, CA, USA). The values were normalized to total protein.

Seahorse assay

Bone marrow-derived macrophages were seeded at a density of 0.5×10^5 cell/well in a XFp plate (Agilent Technologies, Basel, Switzerland) and activated by addition of M1 medium for 24 h. Then, ECAR and OCR were measured as suggested by the manufacturer's protocol for the glycolysis stress test (Agilent Technologies). Briefly, the activated cells were equilibrated in XF base medium (Agilent Technologies) supplemented with 2 mM L-glutamine (Sigma-Aldrich) and placed in a CO_2-free incubator at 37 °C for 1 h prior to the assay. Then, glucose, oligomycin and 2-deoxyglucose (contained in the kit) were sequentially injected in that order during continuous oxygen and H^+ measurements. Data were normalized to cell protein content.

Lactate assay

Lactate was determined in supernatants of M1 macrophages cultured in a 12-well plate at a density of 0.5×10^6 cells/well. Supernatants were collected by snap-freezing 50 μL of sample at each time-point. The samples were measured using the L-lactate assay (Abcam, Cambridge, UK) according to the manufacturer's protocol. Results were normalized to total protein.

Statistical analysis

Statistical analyses were conducted using GraphPad Prism 5.0 software. To analyze the difference between WT and KO, first, the normal distribution of the data was determined using the Shapiro–Wilk normality test. For nonparametric distributed data, the Kruskal–Wallis test followed by the Dunn's posttest was applied. Parametric distributed data were analyzed using an unpaired *t*-test or one-way ANOVA. Values represent mean ± SD.

Acknowledgements

This work was supported by the Swiss National Science Foundation (31003A-159454, 31003A-179400 and 316030-133859). We thank Prof. Gareth G. Lavery, University of Birmingham, UK, for providing the *H6pd* KO mouse line.

Author contributions

PM planned and performed the experiments, analyzed the data and wrote the paper. PK, JB, and DK performed the experiments and analyzed the data. AO planned the experiments, contributed reagents or other essential material, and wrote the paper.

Conflicts of interest

The authors declare that they have no conflicts of interest.

References

1 Sapolsky RM, Romero LM & Munck AU (2000) How do glucocorticoids influence stress responses?

Integrating permissive, suppressive, stimulatory, and preparative actions. *Endocr Rev* **21**, 55–89.
2 Odermatt A & Kratschmar DV (2012) Tissue-specific modulation of mineralocorticoid receptor function by 11beta-hydroxysteroid dehydrogenases: an overview. *Mol Cell Endocrinol* **350**, 168–186.
3 Atanasov AG, Nashev LG, Gelman L, Legeza B, Sack R, Portmann R & Odermatt A (2008) Direct protein-protein interaction of 11beta-hydroxysteroid dehydrogenase type 1 and hexose-6-phosphate dehydrogenase in the endoplasmic reticulum lumen. *Biochim Biophys Acta* **1783**, 1536–1543.
4 Atanasov AG, Nashev LG, Schweizer RA, Frick C & Odermatt A (2004) Hexose-6-phosphate dehydrogenase determines the reaction direction of 11beta-hydroxysteroid dehydrogenase type 1 as an oxoreductase. *FEBS Lett* **571**, 129–133.
5 Ozols J (1993) Isolation and the complete amino acid sequence of lumenal endoplasmic reticulum glucose-6-phosphate dehydrogenase. *Proc Natl Acad Sci USA* **90**, 5302–5306.
6 Ozols J (1995) Lumenal orientation and post-translational modifications of the liver microsomal 11 beta-hydroxysteroid dehydrogenase. *J Biol Chem* **270**, 10360.
7 Beutler E & Morrison M (1967) Localization and characteristics of hexose 6-phosphate dehydrogenase (glucose dehydrogenase). *J Biol Chem* **242**, 5289–5293.
8 Hori SH & Takahashi T (1977) Latency of microsomal hexose-6-phosphate dehydrogenase activity. *Biochim Biophys Acta* **496**, 1–11.
9 Banhegyi G, Benedetti A, Fulceri R & Senesi S (2004) Cooperativity between 11beta-hydroxysteroid dehydrogenase type 1 and hexose-6-phosphate dehydrogenase in the lumen of the endoplasmic reticulum. *J Biol Chem* **279**, 27017–27021.
10 Lavery GG, Walker EA, Draper N, Jeyasuria P, Marcos J, Shackleton CH, Parker KL, White PC & Stewart PM (2006) Hexose-6-phosphate dehydrogenase knock-out mice lack 11 beta-hydroxysteroid dehydrogenase type 1-mediated glucocorticoid generation. *J Biol Chem* **281**, 6546–6551.
11 Tuckermann JP, Kleiman A, McPherson KG & Reichardt HM (2005) Molecular mechanisms of glucocorticoids in the control of inflammation and lymphocyte apoptosis. *Crit Rev Clin Lab Sci* **42**, 71–104.
12 Coutinho AE & Chapman KE (2011) The anti-inflammatory and immunosuppressive effects of glucocorticoids, recent developments and mechanistic insights. *Mol Cell Endocrinol* **335**, 2–13.
13 Amano Y, Lee SW & Allison AC (1993) Inhibition by glucocorticoids of the formation of interleukin-1 alpha, interleukin-1 beta, and interleukin-6: mediation by decreased mRNA stability. *Mol Pharmacol* **43**, 176–182.
14 Kunicka JE, Talle MA, Denhardt GH, Brown M, Prince LA & Goldstein G (1993) Immunosuppression by glucocorticoids: inhibition of production of multiple lymphokines by *in vivo* administration of dexamethasone. *Cell Immunol* **149**, 39–49.
15 Crinelli R, Antonelli A, Bianchi M, Gentilini L, Scaramucci S & Magnani M (2000) Selective inhibition of NF-kB activation and TNF-alpha production in macrophages by red blood cell-mediated delivery of dexamethasone. *Blood Cells Mol Dis* **26**, 211–222.
16 Brewer JA, Khor B, Vogt SK, Muglia LM, Fujiwara H, Haegele KE, Sleckman BP & Muglia LJ (2003) T-cell glucocorticoid receptor is required to suppress COX-2-mediated lethal immune activation. *Nat Med* **9**, 1318–1322.
17 Gordon S (2003) Alternative activation of macrophages. *Nat Rev Immunol* **3**, 23–35.
18 Goerdt S, Politz O, Schledzewski K, Birk R, Gratchev A, Guillot P, Hakiy N, Klemke CD, Dippel E, Kodelja V *et al.* (1999) Alternative versus classical activation of macrophages. *Pathobiology* **67**, 222–226.
19 Stein M, Keshav S, Harris N & Gordon S (1992) Interleukin 4 potently enhances murine macrophage mannose receptor activity: a marker of alternative immunologic macrophage activation. *J Exp Med* **176**, 287–292.
20 Erwig LP, Kluth DC, Walsh GM & Rees AJ (1998) Initial cytokine exposure determines function of macrophages and renders them unresponsive to other cytokines. *J Immunol* **161**, 1983–1988.
21 Fadok VA, Bratton DL, Konowal A, Freed PW, Westcott JY & Henson PM (1998) Macrophages that have ingested apoptotic cells *in vitro* inhibit proinflammatory cytokine production through autocrine/paracrine mechanisms involving TGF-beta, PGE2, and PAF. *J Clin Invest* **101**, 890–898.
22 Thieringer R, Le Grand CB, Carbin L, Cai TQ, Wong B, Wright SD & Hermanowski-Vosatka A (2001) 11 Beta-hydroxysteroid dehydrogenase type 1 is induced in human monocytes upon differentiation to macrophages. *J Immunol* **167**, 30–35.
23 Gilmour JS, Coutinho AE, Cailhier JF, Man TY, Clay M, Thomas G, Harris HJ, Mullins JJ, Seckl JR, Savill JS *et al.* (2006) Local amplification of glucocorticoids by 11 beta-hydroxysteroid dehydrogenase type 1 promotes macrophage phagocytosis of apoptotic leukocytes. *J Immunol* **176**, 7605–7611.
24 Chapman KE, Coutinho A, Gray M, Gilmour JS, Savill JS & Seckl JR (1088) Local amplification of glucocorticoids by 11beta-hydroxysteroid dehydrogenase type 1 and its role in the inflammatory response. *Ann N Y Acad Sci* **2006**, 265–273.
25 Chapman KE, Coutinho AE, Zhang Z, Kipari T, Savill JS & Seckl JR (2013) Changing glucocorticoid action: 11beta-hydroxysteroid dehydrogenase type 1 in acute

and chronic inflammation. *J Steroid Biochem Mol Biol* **137**, 82–92.
26 Haschemi A, Kosma P, Gille L, Evans CR, Burant CF, Starkl P, Knapp B, Haas R, Schmid JA, Jandl C *et al.* (2012) The sedoheptulose kinase CARKL directs macrophage polarization through control of glucose metabolism. *Cell Metab* **15**, 813–826.
27 Schuster D, Maurer EM, Laggner C, Nashev LG, Wilckens T, Langer T & Odermatt A (2006) The discovery of new 11beta-hydroxysteroid dehydrogenase type 1 inhibitors by common feature pharmacophore modeling and virtual screening. *J Med Chem* **49**, 3454–3466.
28 Van den Bossche J, Baardman J, Otto NA, van der Velden S, Neele AE, van den Berg SM, Luque-Martin R, Chen HJ, Boshuizen MC, Ahmed M *et al.* (2016) Mitochondrial dysfunction prevents repolarization of inflammatory macrophages. *Cell Rep* **17**, 684–696.
29 Zhang YL, Zhong X, Gjoka Z, Li Y, Stochaj W, Stahl M, Kriz R, Tobin JF, Erbe D & Suri V (2009) H6PDH interacts directly with 11beta-HSD1: implications for determining the directionality of glucocorticoid catalysis. *Arch Biochem Biophys* **483**, 45–54.
30 Bublitz C & Steavenson S (1988) The pentose phosphate pathway in the endoplasmic reticulum. *J Biol Chem* **263**, 12849–12853.
31 Hino Y & Minakami S (1982) Hexose-6-phosphate and 6-phosphogluconate dehydrogenases of rat liver microsomes. Involvement in NADPH and carbon dioxide generation in the luminal space of microsomal vesicles. *J Biochem* **92**, 547–557.
32 Bublitz C (1981) Physical separation of cytoplasmic and microsomal 6-phosphogluconate dehydrogenases from rat liver. *Biochem Biophys Res Commun* **98**, 588–594.
33 Bublitz C, Lawler CA & Steavenson S (1987) The topology of phosphogluconate dehydrogenases in rat liver microsomes. *Arch Biochem Biophys* **259**, 22–28.
34 Zhang TY & Daynes RA (2007) Macrophages from 11beta-hydroxysteroid dehydrogenase type 1-deficient mice exhibit an increased sensitivity to lipopolysaccharide stimulation due to TGF-beta-mediated up-regulation of SHIP1 expression. *J Immunol* **179**, 6325–6335.
35 Kipari T, Hadoke PW, Iqbal J, Man TY, Miller E, Coutinho AE, Zhang Z, Sullivan KM, Mitic T, Livingstone DE *et al.* (2013) 11beta-hydroxysteroid dehydrogenase type 1 deficiency in bone marrow-derived cells reduces atherosclerosis. *FASEB J* **27**, 1519–1531.
36 Clarke JL & Mason PJ (2003) Murine hexose-6-phosphate dehydrogenase: a bifunctional enzyme with broad substrate specificity and 6-phosphogluconolactonase activity. *Arch Biochem Biophys* **415**, 229–234.
37 Krawczyk CM, Holowka T, Sun J, Blagih J, Amiel E, DeBerardinis RJ, Cross JR, Jung E, Thompson CB, Jones RG *et al.* (2010) Toll-like receptor-induced changes in glycolytic metabolism regulate dendritic cell activation. *Blood* **115**, 4742–4749.
38 Marini C, Ravera S, Buschiazzo A, Bianchi G, Orengo AM, Bruno S, Bottoni G, Emionite L, Pastorino F, Monteverde E *et al.* (2016) Discovery of a novel glucose metabolism in cancer: the role of endoplasmic reticulum beyond glycolysis and pentose phosphate shunt. *Sci Rep* **6**, 25092.
39 Frauwirth KA, Riley JL, Harris MH, Parry RV, Rathmell JC, Plas DR, Elstrom RL, June CH & Thompson CB (2002) The CD28 signaling pathway regulates glucose metabolism. *Immunity* **16**, 769–777.
40 Zhang X, Goncalves R & Mosser DM (2008) The isolation and characterization of murine macrophages. *Curr Protoc Immunol* **83**, 14.1.1–14.1.14. Chapter 14 Unit 14 11.
41 Seibert J, Hysek CM, Penno CA, Schmid Y, Kratschmar DV, Liechti ME & Odermatt A (2014) Acute effects of 3,4-methylenedioxymethamphetamine and methylphenidate on circulating steroid levels in healthy subjects. *Neuroendocrinology* **100**, 17–25.
42 Steinberg BE & Grinstein S (2009) Analysis of macrophage phagocytosis: quantitative assays of phagosome formation and maturation using high-throughput fluorescence microscopy. *Methods Mol Biol* **531**, 45–56.
43 Low H, Hoang A & Sviridov D (2012) Cholesterol efflux assay. *J Vis Exp* **61**, e3810.